Direct Observation of the Electroadsorptive Effect on Ultrathin Films for Microsensor and Catalytic-Surface Control

Theodor Doll,*[a] Juan J. Velasco-Velez,[a, c] Dirk Rosenthal,*[b] Jonathan Avila,[d, e] and Victor Fuenzalida[e]

Microchemical sensors and catalytic reactors make use of gases during adsorption in specific ways on selected materials. Fine-tuning is normally achieved by morphological control and material doping. The latter relates surface properties to the electronic structure of the bulk, and this suggests the possibility of electronic control. Although unusual for catalytic surfaces, such phenomena are sometimes reported for microsensors, but with little understanding of the underlying mechanisms. Herein, direct observation of the electroadsorptive effect by a combination of X-ray photoelectron spectroscopy and conductivity analysis on nanometre-thick semiconductor films on buried control electrodes is reported. For the SnO_2/NO_2 model system, NO_3 surface species, which normally decay at the latest within minutes, can be kept stable for 1.5 h with a high coverage of 15 % under appropriate electric fields. This includes uncharged states, too, and implies that nanoelectronic structures provide control over the predominant adsorbate conformation on exterior surfaces and thus opens the field for chemically reactive interfaces with in situ tunability.

1. Introduction

The effect of electric control on gas adsorption at surfaces was postulated as early as the invention of semiconductor devices, whereby much of the effort spent on electronics development dealt with surface and interface states. In parallel, catalysis made tremendous use of the latter, but the interplay of electronic states on the one hand and geometrical effects on the other with chemical reactivity seemed to be an unsolvable puzzle, because direct examination of either the geometric or the electronic effect was lacking. We present a first study in which semiconductor sensor measurements are coupled with surface analysis on a model system under the dominant electronic effect of electronic surface states control. The results shine light on the molecule–surface interactions, which fit well into an interdisciplinary view based on semiconductor device physics, surface analytical techniques, and the theory of catalysis.

In 1930, Lilienfeld patented a semiconductor structure that laid the basis for later field-effect transistors.[1] The patent postulated the conductivity control of a thin semiconductor layer by means of an external electric field. In 1935 Heil presented a suspended gate structure that should control surface states and hence the conductivity of a thin film by external electric fields.[2] The malfunction of these early structures remained unexplained until 1948, when Shockley and Pearson clarified that only 10 % of the charge carriers in such thin-film arrangements were mobile;[3] surface and interface states dominated all device behaviour. The effort spent on diminishing and saturating interface defects for MOS technology since the mid-1950s is unparalleled, and aid was sought from all neighbouring disciplines. In turn, interdisciplinary insights arose in the manipulation of adsorbed species and their use for gas detection by subsequently developed semiconductor sensors and also in catalysis. For the latter, chemical view, the first quantum mechanical description of coupled solid interface/adsorbate systems was given by Wolkenstein,[4] who in 1958 presented a theory on the influence of electric fields on adsorption and desorption, named the electroadsorptive effect (EAE).[5]

The EAE was experimentally observed, for example, by Keier and Mikheeva in 1964 for methanol on germanium[6] and by Hönig and Lane, who found for O_2 on ZnO[7] clear increases

[a] Prof. Dr. T. Doll,+ Dr. J. J. Velasco-Velez
    Microstructure Physics, University of Mainz
    Staudinger Weg 7, 55128 Mainz (Germany)
    E-mail: dollth@uni-mainz.de

[b] Dr. D. Rosenthal
    Inorganic Chemistry, Fritz-Haber-Institut der Max-Planck-Gesellschaft
    Faradayweg 4–6, 14195 Berlin (Germany)
    E-mail: dirkrose@fhi-berlin.mpg.de

[c] Dr. J. J. Velasco-Velez
    Materials Science Division, Lawrence Berkeley National Laboratory
    Cyclotron Road, Berkeley CA 94720 (USA)

[d] Dr. J. Avila
    Laboratorio de Filmes Finos e Superficies (LFFS), CFM
    Universidade Federal de Santa Catarina
    Caixa Postal 476, CEP 88040-900 Florianópolis, SC (Brasil)

[e] Dr. J. Avila, Prof. Dr. V. Fuenzalida
    Departamento de Física, Universidad de Chile
    Av. Blanco Encalada 2008, Santiago (Chile)

[+] Current address:
    Biomedical Engineering, VIANNA, Hannover Medical School
    Feodor-Lynen-Str. 35, 30625 Hannover (Germany)
    E-mail: doll.theodor@mh-hannover.de

and decreases in adsorption-induced thin-film conductivities under electric fields as strong as 36 kV cm^{-1}. As such fields are too close to the normal discharge limit in air, practical use seemed to be chanceless.

Also, in the 1970s, the field of catalysis was concerned with the EAE, because it was found that semiconductor doping levels could not influence apparent activation energy levels. Ertl and Gerischer pointed out that field effects could still enhance reactivities if charged adsorbates were more reactive than uncharged ("weak") ones.[8] However, any studies at this time were hampered by surface impurities. In turn, morphological aspects evolved as the prevailing paradigm of the field.

On the electronics side, conditions changed with the advent of micro- and nanotechnological devices, in which, on the one hand, drops of several volts across a few or tens of nanometres show that insulators can bear extreme electric strengths. On the other hand, semiconducting thin films for chemical sensing became available with greatly improved purities. Hence, since the 1990s the EAE and Wolkenstein's theory were revived by several findings on semiconductor gas microsensors[9–14] and nanosensing.[15,16]

Nevertheless, the detailed mechanisms that govern surface reactions in the presence of external electric fields remained not entirely understood. Also, details on the surface states involved are sparse, as most observations stem from indirect measurements. In this study we add direct surface analysis to semiconductor measurements. As the material, we chose tin oxide layers because of the vast knowledge of their semiconductor sensing properties.[17,18] Similar reasoning suggested the use of NO$_2$ for test reactions.[19–23] During and after exposure to high electric fields, chemical analysis of adsorbates and characterization of the underlying semiconductor were performed, and both measurements are discussed on the basis of an extended Wolkenstein model.

2. Results and Discussion

2.1. X-ray Photoelectron Spectroscopic (XPS) Measurements

The XPS analysis was started a few minutes after exposing compact or porous SnO$_2$ layers to NO$_2$/O$_2$ mixtures. The N 1s photoelectron signal showed peaks at binding energies of 406 and 408 eV, related to chemisorbed NO$_2$ and NO$_3$, respectively.[23–25] The peaks at 400 and 399 eV are associated with Sn—NO$_{ad}$ and nitrogen replacing oxygen in the crystal lattice.[26–28] The latter peaks around 400 eV appear after exposure of freshly prepared films to NO$_2$ and remain stable for days, in contrast to the peaks of NO$_2$ and NO$_3$.

As both the compact and the porous layers show very similar adsorption characteristics (besides the total amount of adsorbed gas and its desorption over time, see the Experimental Section), the average of a series of 70 measurements was calculated and is presented as a schematic reconstruction of the porous and compact layers in Figure 1. For zero voltage (see the Supporting Information), we find NO/N to be the dominant stable species with partial coverages of 54%. Both NO$_2$ and NO$_3$, which start at about 28 and 18% coverage, respectively,
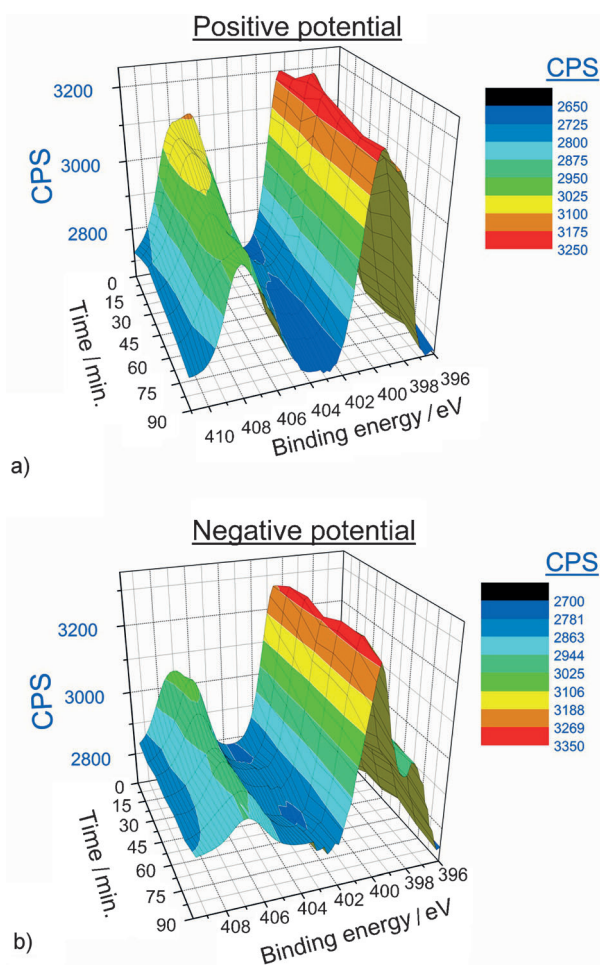

Figure 1. Reconstruction of the XPS results of the porous and compact layers: Development of the N 1s peak (400 eV binding energy) over time under positive (a) and negative (b) bias. The peaks arising at 406 and 408 eV correspond to NO$_2$ and NO$_3$, respectively.

fade away during our 90 min period of observation with decay times of 40 min (porous) and 25 min (compact).

Figure 1 shows the averaged N 1s photoelectron signals as a function of time for positive and negative polarization. Figure 1a reveals that, under positive applied potentials (negative electric fields), the NO$_2$ peak reaches 80% of the signal height of the NO/N species and decays much more slowly over time. The NO$_3$ species become only slightly pronounced, but their stability over time is clearly enhanced. In total we find stabilisation and intensification of the NO$_2$/NO$_3$ configuration under positive potentials.

On the other hand, application of a negative potential (positive electric field) stimulates desorption of NO$_2$ and NO$_3$ from the SnO$_2$ surface (Figure 1b). NO$_3$ is almost entirely missing after the short transfer period. NO$_2$ starts at similar values as under zero voltage (50% relative peak height) but decays more quickly. In addition, we find an increase of the NO/N peak over time for the porous layer (see the Supporting Information) that clearly surmounts the porosity effects discussed below.

Changes may partially arise from bias-dependant inner diffusion of interstitial nitrogen species inside the bulk by means of

a driving force (electric field). Application of a positive voltage induces accumulation of Sn–N states at the surface. Vice versa, a negative potential results in diffusion of N into the bulk and reduces the concentration at the surface. This is confirmed by other studies based on angle-resolved XPS (AR-XPS), which provides chemical information on the surface and the bulk (thickness < 6 nm).[29]

These findings provide explicit evidence on the electric desorption control of chemisorbed species. As a general trend the pronounced desorption under negative potentials comes in parallel with some increase in lattice nitrogen (i.e. Sn–O–N), which is higher for the rougher evaporated thin films. In contrast, under positive voltages, desorption is strongly suppressed. The same conclusion is supported by reassessing the N 1s intensities with respect to those of C 1s.

The energy split between NO_2 (406 eV) and NO_3 (408 eV) is wide enough to identify both species univocally. The peak areas of the two single components are shown in Figure 2, which shows that the applied voltage drastically affects desorption of the NO_3 species. Whereas positive polarization suppresses desorption during the period under study, negative polarization causes rapid desorption of NO_3 in comparison to NO_2.

Beneath desorption another process is very likely to happen; the increase in NO (or N) species amounts to 6 % peak height according to Figure 1 for negative voltages. As surface N undergoes bulk diffusion, it must originate from a conformational change of other adsorbed species. This may be NO_3 (or NO_2), which is seen from Figure 2 to drop by at least 30 % even in the positive case. The XPS intensities show that about 20 % of NO_3 (or NO_2) is transformed whilst the remainder is lost by desorption.

2.2. Conductivity Measurements

The electrode configurations in our test devices allow for simultaneous read-out of the field effect inside the semiconductor thin film. Hereby, purely voltage dependent electronic processes are superimposed by gas-sensitive effects that depend nonlinearly on the amount of adsorbed species. Their surface states can be charged according to the adsorption-modified surface statistics, which in turn is ruled by the bulk Fermi level.

The change in conductivity due to adsorbed gases is related to the formation of a space-charge region adjacent to the surface. The biasing electric field produces a second space-charge region that arises at the buried insulator/semiconductor interface (see inset of Figure 3). An appropriate biasing field will control both the device conductivity and the adsorption/desorption at the metal-oxide surface. For the electric field to reach the surface, the space-charge region must cross the whole semiconductor thickness, whilst for measurable conductivity one path parallel to the surface must remain at the same time.

Figure 3 shows the conductivities recorded during the XPS experiment. According to normal transistor operation (−30 to 22.5 min) we find a higher current under positive voltages,
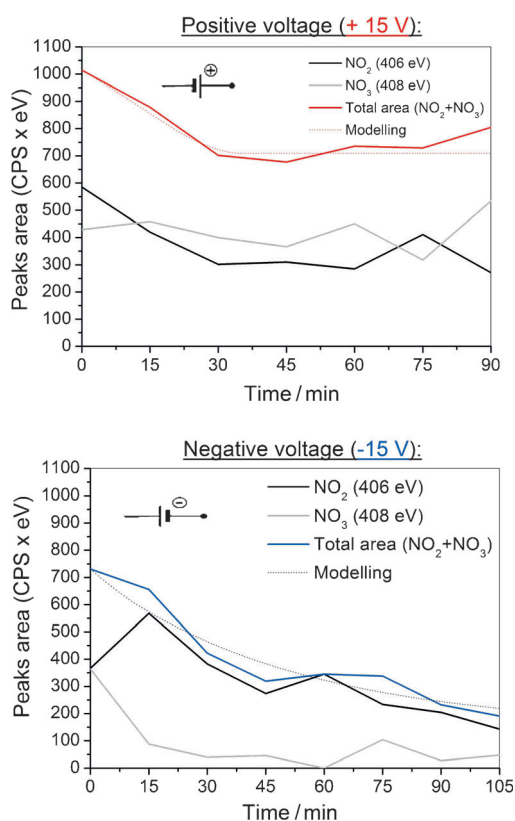

Figure 2. Time dependence of peak areas (porous sample) of NO_2 (406 eV) and NO_3 (408 eV) under polarization at positive voltage (left) and negative voltage (right). The red/blue lines are the total peak area (NO_2 and NO_3). The dotted line reflects our modelling results.
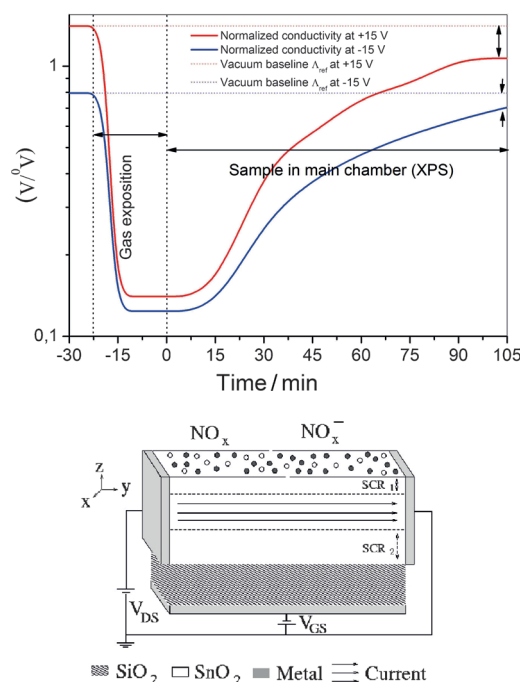

Figure 3. Conductivity (porous sample) related to the presence of NO_x at positive voltage (+ 15 V) and at negative potential (−15 V). Dotted lines show the reference conductivity in absence of gases (baselines). Inset: Thin-film transistor model device.

which means that the backward end of the space charge is diminished and the conducting path is widened. The effect of negative voltages runs vice versa.

For exposure to NO_2 a general decrease in conductivity fits the oxidative nature of NO_2: Formation of NO_x^- acceptor surface states, widening of the space-charge region and, as a result, a narrowed conductive path. The time constants agree well with other findings for room-temperature metal oxides.[30] The response under biasing voltage differs both in absolute and relative measures. Whilst the absolute values are relevant for catalysis, as the total number of ionized adsorbates is changed, the relative changes count for sensor applications. For positive voltages the absolute (relative) change amounts to 1.35 a.u. (10). For negative bias 0.67 a.u. (6) is obtained. For the decay back to the baselines we find also a faster desorption for negative bias voltages, consistent with XPS intensities.

3. Conclusions

The surface species for adsorption of NO_2 on SnO_2 are consistent with the findings of Maiti et al.,[23] which were extended towards their control under electric fields. We observed a strong dependence of adsorption/desorption of NO_3 species on electric field, with almost on/off characteristics. In general, one can assume that both NO_2 and NO_3 states may be present in charged and uncharged states at the surface, and both are under the control of the electric field. Since, due to the Weisz limit,[31] the 30% increase observed cannot all stem from charged species, we conclude that uncharged states are also controlled by the electric field. If the Wolkenstein model is combined with the appropriate Shockley–Read–Hall statistics and literature parameters are used, also the dynamic behaviour of the coverages of the latter species can be well described, as is depicted in Figure 2 (••••, modelling). We find that the electroadsorptive effect influences the total amount of adsorbed NO_x. Its coverage is enhanced under positive voltages and adsorbates stay there longer. Thus, for surface reactions more NO_x is available and, in particular, if a desired reaction requires the NO_3 conformation, the EAE can promote such reactions. More importantly, two different (polycrystalline) surface morphologies yield similar results. Thus the EAE offers a vital approach for catalytic surface optimization independent of morphological strategies.

With regard to semiconductor sensor applications we find that the potential for using the EAE is more limited, because only charged adsorbates are directly observed under electronic readout. However, counteractions with other adsorbates may play important roles, too. The role of residual coadsorbed oxygen

and water are still not considered, and existing onsets[32] of a multi-surface-state modelling will need substantial data.

One approach towards them would be in situ experiments, for example, by AP-XPS and X-ray absorption spectroscopy. The former offers the opportunity to reach pressures in the range of several tens of torr, which are sufficient for our requirements. On the other hand, secondary electrons collected in the sensitive layer may provide information on the interface between solid and gas under ambient pressure conditions. Such measurements are planned in a high-pressure gas cell with mixtures of various gases.

Experimental Section

Device: A sensor-like semiconductor nanofilm setup was designed for direct observation of the EAE by X-ray photoelectron spectroscopy (XPS). For required high field strengths and bare surfaces, a buried control electrode underneath the layer was chosen. Thus, the device is similar to a film transistor. Using layer thicknesses in the range of several Debye lengths L_D[33] ensures that the rear electric field penetrates the entire layer and reaches the front surface. For the sensitive metal oxide layer we chose SnO_2 with an L_D value of approximately 40 nm at room temperature. NO_2 was selected as model gaseous adsorbate due to the vast amount of data reported on the NO_2/SnO_2 system.

The device is shown in Figure 4. For the back (buried) electrode a silicon n+ chip was used with silicon oxide as insulating layer towards the frontal SnO_2 thin layer. Small silver or gold lines at the rim of the SnO_2 serve for 1) electrical grounding of the surface and 2) conductivity measurement on the layer. Also shown are the band diagrams for two states of operation: positive or negative back-electrode voltage. For positive voltages, the electron energy of the electrode is lowered and the resulting electric field tilts the insulator bands upwards. The bands of the semiconductor layer are not tilted due to the occurrence of Fermi level pinning for thicknesses in the L_D range. However, the Fermi level is shifted upwards and extra negative charge is created. This affects the surface states, too, which become increasingly charged, as they are acceptor-type in our case. For negative backside voltages the scheme runs vice versa and the uncharged surface states prevail.
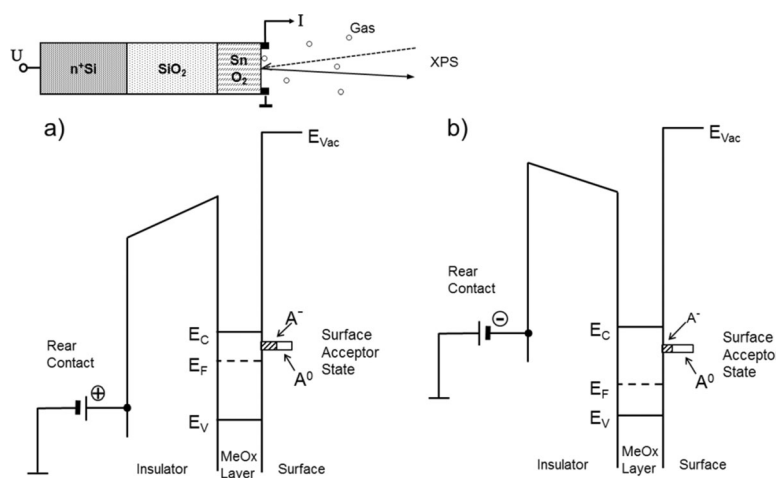

Figure 4. Theory of adsorption behaviour of the back-electrode insulator/semiconductor structure. a) Positive potential induces adsorption of charged species (A^-); A^0 refers to neutral species (not charged). b) Negative potential induces their desorption.

The potential of the buried electrode determines the position of the Fermi level E_F, which governs the surface-state statistics and hence the reaction probability. If only one adsorbed species is present, the main effect of the electric field is to alter the charging probability of adsorbates, which under ambient conditions is less than 1% (Weisz self-limitation).[31] However, if competitive adsorption of several gases is involved, the final result will depend on the availability of free adsorption sites and hence the various binding strengths and partial gas pressures.

With regard to frequent discussions, we wish to clarify that, due to the presence of electronically vacant surface states, no electric field leaves the frontal surface. As its rim has been electrically tied to ground, no charging effects are superimposed on the XPS measurements. This was carefully cross-checked with C 1s calibration and the other O 1s and Sn 3d peaks. Thus, the entire surface band structure including the core levels was grounded, too. The surface states can either fade away in terms of existence (no adsorbed molecule in a specific conformation = no state), or their electronic occupation statistics can be changed by the Fermi level, which is altered by the backward field. Additionally, if one adsorbed molecule is able to change its conformation (in our case, NO can transform itself into the states NO_2 and NO_3 by consuming adjacent atoms), one surface state disappears and reappears at another position within the band gap. In XPS field-dependent chemical shifts are observed on a quasi-neutral background, as the probing depth of XPS is much smaller then the width of the space-charge region.

The SnO_2 layer was deposited by Ar/O_2 radio-frequency RF sputtering from a SnO_2 target followed by annealing in dry synthetic air (400 °C/100 h) or by e-beam evaporation from pure Sn with humid-air oxidation (400 °C/24 h). The resulting oxide layers were 100 nm thick and had an intrinsic doping level of approximately 10^{18} cm^{-3} oxygen vacancies according to measurements on identically prepared layers.[34] The insulator thickness varied from 1 μm (sputtering) to 100 nm (e-beam). A TEM investigation on the sputtered structures showed that the devices had compact layers with crystallite domains ranging from 5 to 25 nm and missing texture and surface faceting (see Figure 5). Thus gas diffusion along grain boundaries of the sputtered samples is rather unlikely. The layer can be considered as amorphous in terms of X-ray analysis. The evaporated samples, however, had high surface roughness and a thickness ranging from 20 to 100 nm. An energy-dispersive X-ray analysis showed a stoichiometry that was sufficient for a doping concentration ensuring the Debye criteria for functioning of the effect.

Two major differences between porous and compact layers were observed. First, the XPS Sn–N lattice peak was far more prominent in the evaporated samples, which may be due to residual gas pressures of 5×10^{-6} mbar during deposition. Second, the porous samples showed slightly increased surface coverages during analysis (up to 6% over time), whereas the compact layers had (normal) overall decays. The increases were found to be voltage-insensitive and were attributed to relocation of adsorbed species from pores and grain boundaries. By combining data for both porous and compact layers, these differences are suppressed and the pure EAE effect is highlighted.

Gas Exposure: A vacuum setup with a separate gas-exposure chamber connected though sample transfer to the XPS measurement chamber was used to allow continuous electrical control during manipulation. An NO_2/O_2 mixture (80/20%) was internally produced by heating lead nitrate with mass-spectrometric monitoring. The devices, stored under ultra-high vacuum (UHV), were exposed for 10 min at 10^{-3} mbar. Within 3 min after restarting HV pumping the devices were pushed into the main UHV chamber and the XPS time series was started. Therefore, no measurements for $t = 0$ are available, and rapidly desorbed species are excluded from observation. To a first approximation, in HV systems, the stronger the binding of previously adsorbed molecules, the longer they stay at the surface. Beneath pre-/coadsorbed oxygen and water, residual NO, NO_2 and NO_3 species (i.e. NO_x) as well as interstitial nitrogen can be identified by XPS regardless of their possible charges. Following the results of Rodriguez et al. on TiO_2[24] we expect that chemisorbed NO_2 will either decompose to give NO_{ad} and O_{ad} or disproportionate to give NO_3 and NO. Figure 6 depicts
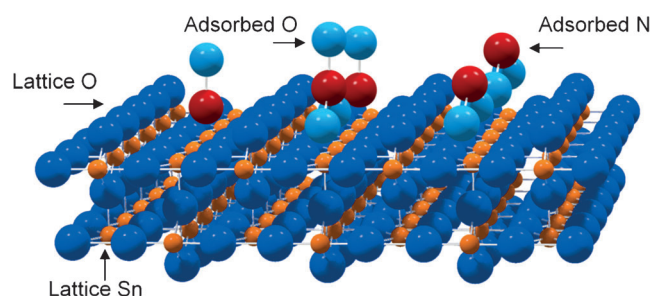

Figure 6. Most common SnO_2 (110) surface after adsorption of NO_2 from the gas phase with NO, NO_2 and NO_3 species. Lattice O and Sn atoms as well as O and N atoms in adsorbed species are marked by arrows.
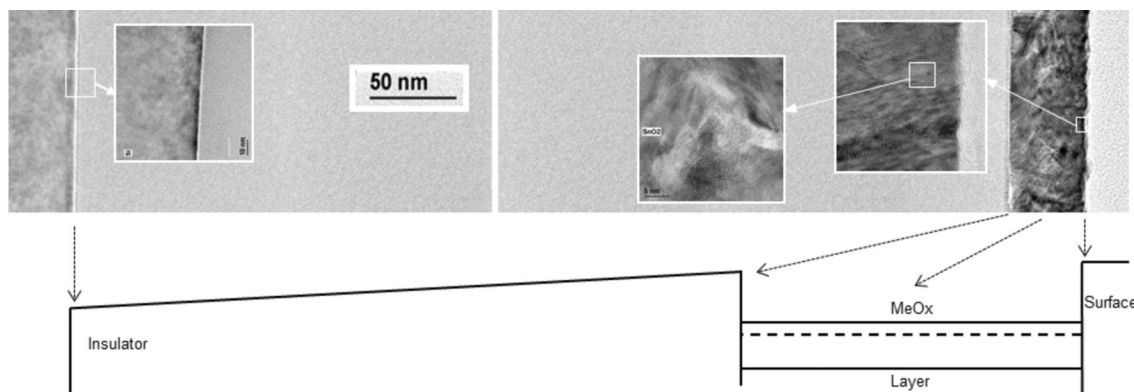

Figure 5. TEM cross section of the entire device structure. Buried silicon electrode (left), Si_3N_4 insulator (140/250 nm) and SnO_2 sensing layer (right). The high-resolution image of the sensing layer shows the compact structure and approximate grain size of 5–25 nm. No preferential orientation is present.

the preferred sites of these adsorbates on the (110) SnO_2 surface plane, which is the most common facet on polycrystalline surfaces[17] with quasi-amorphous blurring of defects.

Modelling: The Wolkenstein–Geistlinger model[4,5,35,36] formulates a Fermi-level-dependent adsorption coefficient β that is multiplied by the partial pressure in a standard Langmuir isotherm. The model takes into account the quantum chemistry of chemisorption wherein physisorption is considered as an independent precursor of two chemisorbed states ("strong" and "weak"). In this view the weak state remains uncharged and, in terms of charging, is not different from the physisorbed state, which, however, has a different (i.e. smaller) binding energy. Weak and strong states are both governed by the Fermi level. As the position of the surface states is referenced to the vacuum level, both states are sensitive to electric field through the surface band bending ΔV_S, but only the charged ones are electrically detected. With two space-charge regions (bulk and front), the electrical conductance G can be described as $G = \sigma_0(W/L)(d - SCR_b - SCR_f)$, in which W and L are width and length, σ_0 is the bulk conductivity, d the layer thickness and SCR denotes the depth of a space-charge region. SCR_b is purely electronic, and SCR_f is gas-sensitive and electronically influenced. For the sought dynamic response the Wolkenstein isotherm was combined with Shockley–Read–Hall statistics,[31,32,37] which describes the temporal fluctuations of charged adsorption by means of capture processes. For example, the desorption of charged, "strongly" chemisorbed adsorbates is described by a capture coefficient K_n that rules over the remaining "weakly" adsorbed ones $N^0 = (N - N^-)$ with electron transitions from the surface conduction band E_{cs} and desorption from the adsorption levels described as trap states E_t [Eq. (1)]:

$$\frac{dN^-}{dt} = K_n \left[(N - N^-)N_c \exp\left(-\frac{E_{cs} - E_F}{kT}\right) - N^- N_c \exp\left(-\frac{E_{cs} - E_t}{kT}\right) \right] \tag{1}$$

The results of such modelling[38] are shown as a segmented line in Figure 2, which exhibits fair agreement of observed time and voltage dependence with modelling of the total sum of weakly and strongly chemisorbed NO_x^0 and NO_x^- particles. The time constants of XPS as well as conductivity measurement and modelling lie within the same range. This indicates that the charged molecules are present as a constant portion of the entire adsorbates or, to put it the other way around, the electric field governs the uncharged, "weak" states in just the same manner. That, in addition, the total sum of adsorbed nitrogen is controlled by the voltage, however, exceeds such modelling.

Acknowledgements

[1] J. S. E. Lilienfeld, US 1745175, **1930**.
[2] O. Heil, GB 439457, **1934**.
[3] W. Shockley, G. L. Pearson, *Phys. Rev.* **1948**, *74*, 232–233.
[4] T. Wolkenstein, *The Electron Theory of Catalysis on Semiconductors*, Pergamon, Oxford, **1963** (translated, revised version from Russian original).
[5] F. F. Wolkenstein, W. B. Sandomirski, *Dokl. Akad. Nauk SSSR* **1958**, *118*, 980–982.
[6] E. P. Mikheeva, N. P. Keier, *Kinet. Katal.* **1964**, *5*, 748.
[7] S. A. Hoenig, J. R. Lane, *Surf. Sci.* **1968**, *11*, 163–174.
[8] G. Ertl, H. Gerischer in *Physical Chemistry, Vol. X* (Ed.: W. Jost), Academic Press, New York/London, **1970**.
[9] L. I. Popova, S. K. Andreev, B. K. Guoerguiev, N. D. Stoyanov, *Sens. Actuators B* **1994**, *19*, 543–545.
[10] W. Hellmich, G. Müller, C. Bosch-von Braunmühl, T. Doll, I. Eisele, *Sens. Actuators B* **1997**, *43*, 132–139.
[11] M. Hausner, J. Zacheja, J. Gerblinger, J. Binder, DE 4442396 A1, **1996**.
[12] U. Storm, O. Bartels, J. Binder, *Sens. Actuators B* **2001**, *77*, 529–533.
[13] M. Jaegle, J. Wöllenstein, T. Meisinger, H. Böttner, G. Müller, T. Becker, C. Bosch-von Braunmühl, *Sens. Actuators B* **1999**, *57*, 130–134.
[14] M. S. Arnold, P. Avouris, Z. W. Pan, Z. L. Wang, *J. Phys. Chem. B* **2003**, *107*, 659–663.
[15] Z. Y. Fan, J. G. Lu, *Appl. Phys. Lett.* **2005**, *86*, 123510.
[16] P. Andrei, L. L. Fields, J. P. Zheng, Y. Cheng, P. Xiong, *Sens. Actuators B* **2007**, *128*, 226–234.
[17] M. Batzill, U. Diebold, *Prog. Surf. Sci.* **2005**, *79*, 47–154.
[18] A. Gurlo, *ChemPhysChem* **2006**, *7*, 2041–2052.
[19] M. Epifani, J. D. Prades, E. Comini, E. Pellicer, M. Avella, P. Siciliano, G. Faglia, A. Cirera, R. Scotti, F. F. Morazzoni, J. R. Morante, *J. Phys. Chem. C* **2008**, *112*, 19540–19546.
[20] A. Karthigeyan, R. P. Gupta, M. Burgmair, S. K. Sharman, I. Eisele, *Sens. Actuators B* **2002**, *87*, 321–330.
[21] M. Law, H. Kind, B. Messer, F. Kim, P. Yang, *Angew. Chem.* **2002**, *114*, 2511–2514; *Angew. Chem. Int. Ed.* **2002**, *41*, 2405–2408.
[22] T. Yoshida, N. Ogawa, T. Takahashi, *J. Electrochem. Soc.* **1999**, *146*, 1106–1110 and references therein.
[23] A. Maiti, JA. Rodriguez, M. Law, P. Kung, JR. McKinney, P. Yang, *Nano Lett.* **2003**, *3*, 1025–1028.
[24] J. A. Rodriguez, T. Jirsak, G. Liu, J. Hrbek, J. Dvorak, A. Maiti, *J. Am. Chem. Soc.* **2001**, *123*, 9597–9605.
[25] J. A. Rodriguez, T. Jirsak, J. K. Kim, J. Z. Larese, A. Maiti, *Chem. Phys. Lett.* **2000**, *330*, 475–483.
[26] S. S. Pan, C. Ye, X. M. Teng, H. T. Fan, G. H. Li, *Appl. Phys. A* **2006**, *85*, 21–24.
[27] M. Xing, J. Zhang, F. Chen, *Appl. Catal. B* **2009**, *89*, 563–569.
[28] Z. Zhai, K. Zou, W. Feng, Q. Wang, *Mod. Appl. Sci.* **2010**, *4*, 95–100.
[29] K. Takasaki, K. Irino, T. Aoyama, Y. Momiyama, Y. Nakanishi, Y. Tamura, T. Ito, *Fujitsu Sci. Tech. J.* **2003**, *39*, 40–51.
[30] A. Helwig, G. Müller, G. Sberveglieri, M. Eickhoff, *Journal of Sensors* **2009**, 620720.
[31] B. Weisz, *J. Chem. Phys.* **1953**, *21*, 1531–1538.
[32] J. J. Velasco-Velez, C. Wilbertz, T. Haas, T. Doll, *Procedia Chem.* **2009**, *1*, 642–645.
[33] T. Doll, *Advanced Gas Sensing: The Electroadsorptive Effect and Related Techniques*, Kluwer, Boston, **2003**.
[34] A. Oprea, E. Moretton, N. Bârsan, W. J. Becker, J. Wöllenstein, U. Weimar, *J. Appl. Phys.* **2006**, *100*, 033716.
[35] H. Geistlinger, *Surf. Sci.* **1992**, *277*, 429–441.
[36] J. J. Velasco-Vélez, U. Kunze, T. Haas, T. Doll, *Phys. Status Solidi A* **2010**, *207*, 924–929.
[37] W. Shockley, W. T. Read, *Phys. Rev.* **1952**, *87*, 835–842.
[38] $E_F = E_F$ (V_G, back electrode voltage); E_{CS} (conduction band limit at surface) $- E_F = 0,0375$ eV as calculated; $E_C - E_t = 0.03$ eV according to S. Samson, C. G. Fonstad, *J. Appl. Phys.* **1973**, *44*, 4618–4621. $K_n = 10^{-13}$ m³ s⁻¹. The effective density of states in the conduction band is $N_C = 2 M_C (2\pi m_e^* kT/\hbar^2)^{3/2}$ with M_C being the number of band minimums and m_e^* the electron effective mass in the surface states.